

Article

Long-Term Stability of Low-Pressure Reverse Osmosis (RO) Membrane Operation—A Pilot Scale Study

Hyung-Gyu Park and Young-Nam Kwon *

School of Urban & Environmental Engineering, Ulsan National Institute of Science and Technology (UNIST), Ulsan 689-798, Korea; hkpark@unist.ac.kr

* Correspondence: kwonyn@unist.ac.kr; Tel.: +82-52-217-2810

Received: 13 December 2017; Accepted: 18 January 2018; Published: 23 January 2018

Abstract: Reverse osmosis (RO) elements operating at a low pressure (LP) or a low energy (LE) are generally called “LPRO” or “LERO”, and the nomenclature “LP” and “LE” are convertible due to the interrelated features of the pressure and the energy in the RO process. Not only can LPRO be operated at lower pressures, which enables energy saving, but also at the standard operating pressure with an enhanced permeate flux. In this study, the feasibility of the LPRO element was evaluated in the face of high fouling potential feed water. The commercially available standard RO and LPRO were chosen, and the membrane properties including the fouling susceptibility and the surface characteristics were thoroughly evaluated. The variations of various performance parameters were monitored during an 872 h operation in a pilot system, which was operated in a constant flux mode. Then, the used membranes were analyzed to further verify the fouling load localization and the fouling intensities. The average flux variation of the individual RO elements in a vessel and the economic feasibility of LPRO were also evaluated through a simulation study using an RO system design software. This study showed that the localization of fouling load within a pressure vessel of an LPRO system caused about 20% higher flux decline and almost 2-times higher salt passage than those of a standard RO membrane system. Furthermore, the simulation study predicted that average operating pressure difference ratio (%) between two RO membranes decreased from 24.4% to 17.8% and a substantial quantity of LPRO elements (83.3%) must be replaced to meet the designated water criteria only after 2 years’ operation.

Keywords: polyamide RO; fouling; low-pressure RO membrane; RO system simulation

1. Introduction

Reverse osmosis (RO) is a representative demineralization process for which a semipermeable membrane is adopted to remove the dissolved substances from a solution. Liquid and only the marginal portion of some ions can pass to the permeate side through a semipermeable membrane, but the majority of the dissolved materials are rejected. The RO membrane process has been regarded as one of the most economically advantageous separation technologies for both seawater desalination and the purification of various water resources contaminated with pesticides, pharmaceuticals, heavy metals, or other emerging micropollutants. Along with food and beverage processing, the RO process can also be used for recycling wastewater and reclaiming highly valuable resources from the various industrial waste streams. The design and operation of the RO process are relatively simple compared with the other traditional separation processes. The simultaneous achievement of the separation and concentration for diverse compounds is another merit of the RO process.

However, the RO process is still subject to numerous demands including the reduction of the operation and maintenance costs [1–10], prolonging the membrane lifetime [7–17], and advancing the

membrane module and system configuration designs [7,8,18]. The development of a low-pressure (higher flow rate) RO membrane could accomplish some of these demands. Low-pressure RO elements that can be operated at low pressures such as 7.5 bar have been developed for energy saving [19]. Furthermore, ultra-low-pressure RO elements that can be used at much lower operating pressures such as 3 bar to 5 bar were also developed [8,20,21]. With the advances in the membrane performance, the portion of RO element cost in RO systems has simultaneously decreased [7–9,19]. However, despite the recent noticeable progress in the membrane performance, the membrane still suffers from the membrane fouling that is an accumulation of various contaminants on the membrane surface. Fouling by such a build-up of organic contaminants can cause irreversible damage to the membrane surface, which can deteriorate the membrane performance during the system operation, eventually leading to a shortening of the membrane lifetimes [10,14,15,22–28]. The application of LPRO can be also limited by the membrane fouling. It has been long believed that the LPRO membranes cause the decrease in operation pressure and a slight increase in salt passage when operating in constant flux mode. Furthermore, the lower pressure operation of LPRO membranes also has been considered favorable with respect to mitigation of membrane fouling. However, the unevenness of flow rate among individual elements in a pressure vessel might be more intensified in LPRO due to its inherently higher permeability. As a result, there can be a significant difference in the long-term operational stability, especially the membrane fouling susceptibility, between standard and LPRO membranes. In addition, more severe fouling can be generated at higher permeate water flux and lower crossflow velocity [29–32].

Norberg et al. investigated the fouling resistance of commercial LPRO membranes using a feed solution with high organic contents and total dissolved solids [33]. Several pieces of research on the development of fouling-resistant LPRO membrane were also conducted by the modification of membrane surface [34–38]. Furthermore, Huang et al. suggested the necessity of more advanced pretreatment process to prevent membrane fouling occurrence in the LPRO membrane adopted water treatment system [20]. However, few studies were conducted by directly comparing the variations of both system performance and individual elements performance between standard and LPRO membranes in a pilot scale.

The objective of this study is the evaluation of the feasibility of the LPRO elements through the performance of a long-term pilot test wherein feed water with a high fouling potential is adopted. Two types of RO element with different permeate flow rates were chosen for the pilot test. At first, the basic membrane properties including the fouling resistance and the surface characteristics were evaluated and compared to investigate the similarity of physico-chemical properties between the two membranes. Then, the performance variation of the RO systems installed with the two different types of RO element was monitored during the entire test period (872 h). The feed pressure, normalized permeate flow rate (NPF), and normalized salt passage (NSP) were monitored as the representative performance parameters during the pilot test. The performances of the individual RO elements in the pressure vessels were also measured and compared to verify the fouling load localization after the completion of the pilot test. The membrane coupons and the foulants extracted from the used RO elements were investigated to evaluate the fouling behavior according to the permeate flow rates of the RO elements. Furthermore, the average flux variation of the individual RO elements in a vessel and the economic feasibility of LPRO were evaluated through the simulation study using the RO system design software CSMPro 5.0 (Toray Chemical Korea Inc., Seoul, Korea). Especially, the design software input variables including the annual flux decline and the annual salt passage increase were adjusted through the adoption of the pilot test results obtained in this study, thereby enabling the evaluation of the economic feasibility of an LPRO operation that faces high fouling potential feed water.

2. Materials and Methods

2.1. Scheme of the Long-Term Pilot Test

The RO test system, equipped with two parallel sets of pressure vessels and located in A Steel (Dangjin City, Korea), was used for the pilot test study. The schematic of the pilot test apparatus is shown in Figure 1, and the test system is the same as that of the previous study with the exception of the retentate recycling loop [18]. The pilot RO system operation was conducted with an identical feed facing mode that enabled the separate parallel assessments of the two pressure vessels, and each vessel was installed with RO elements comprising different permeate flow rates. Each pressure vessel contained three commercial 8-inch diameter RO elements in a series manner, and the individual RO elements possessed an effective membrane area of 400 square feet.

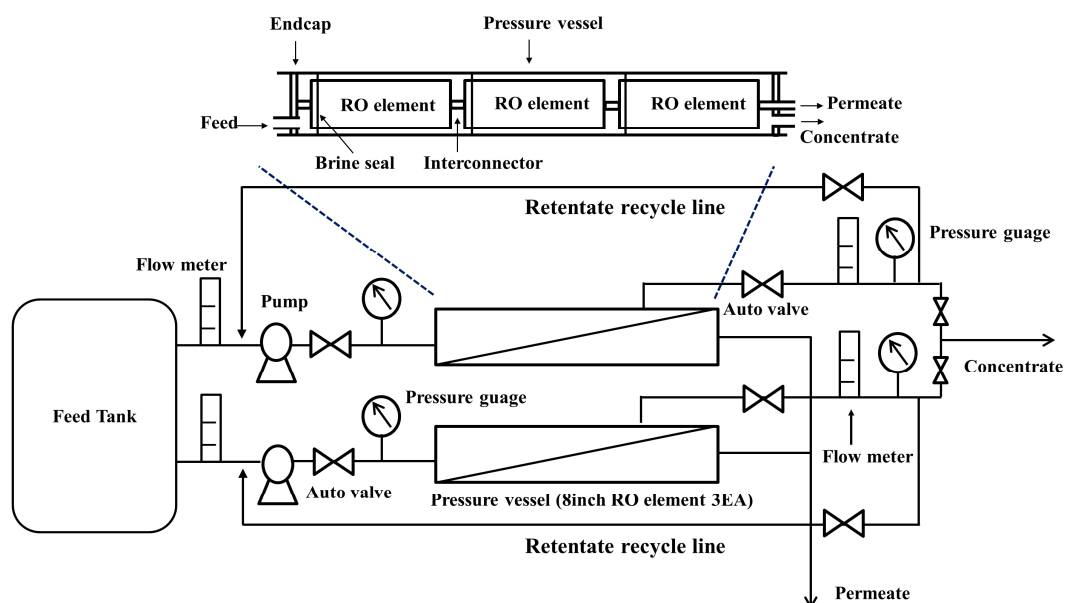


Figure 1. Schematic diagram of mobile long-term test machine.

The LPRO elements 8040-FLR (FLR) were installed in vessel A, and the regular brackish water RO (BWRO) elements 8040-FEn (FEn) were installed in vessel B. Both FLR and FEn are representative fouling resistant RO elements of Toray Chemical Korea Inc. The effective membrane area, element construction materials, and other RO element manufacturing conditions are maintained as the same for the RO elements in vessels A and B, with the membrane performance being the only exception. More detailed descriptions of the test condition, monitoring parameters, and element specifications are described in Table 1. As can be seen in Table 1, considering the different standard test conditions of both RO elements, the LPRO FLR exhibited a higher permeate flow rate than the regular grade RO FEn. The permeate flow rate difference between the two elements is more intensively explained in the subsequent section.

Table 1. Detailed descriptions on the reverse osmosis (RO) elements and monitoring parameters.

RO Element Specification & Evaluation Parameters		
Element specification	Pressure vessel A	RE8040-FLR (9000GPD/99.6%) ^a 3EA
	Pressure vessel B	RE8040-FEn (10,500GPD/99.7%) ^b 3EA
Operation conditions	Permeate (m ³ /h)	2.2 m ³ /h (1 pressure vessel)
	Recovery (%)	33%
	Feed (m ³ /h)	6.5 m ³ /h (1 pressure vessel)
Monitoring parameters	Conductivity (μS/cm)	Feed, Permeate, Retentate
	Pressure (bar)	Feed, Permeate, Retentate
	Feed water quality	Temperature, pH, SDI, Individual ion concentration, TDS

Notes: ^a, ^b Specification of commercially available 8-inch diameter fouling resistant low pressure reverse osmosis (LPRO) and regular grade RO elements manufactured by Toray Chemical Korea Inc.; ^a Low pressure RO (FLR) standard test condition: 1500 ppm NaCl, 10.3 bar, 15% recovery, 25 °C, pH 6.5–7.0; ^b Regular grade RO (FEn) standard test condition: 2000 ppm NaCl, 15.5 bar, 15% recovery, 25 °C, pH 6.5–7.0.

2.2. Monitoring Parameters in the Pilot Test

The pilot RO system was operated under the pressure variation mode where the flux and recovery are maintained as constant. Consequently, the system performance fluctuation led by the fouling was evaluated through the monitoring of the variations of the operating feed pressure, NPF, and NSP.

The data normalization in the RO process is a widely-used calculation method to express the measured system performance from the perspective of the predetermined reference condition. The inevitable variations in the operating conditions may cause fluctuations in the permeate flow rate and the salt passage, which prevent the detection of the performance deteriorations due to the membrane property changes. The data normalization allows the operator to determine whether the noticeable variations in the system performance (flow rate and/or salt passage) are normal alterations caused by the changes in the operating conditions, or indicative of fouling, scaling, and/or membrane integrity loss. In this regard, NPF is the most influential monitoring parameter for the RO system, where factors including the pressure, temperature, and solute concentration variations are considered. The NPF could therefore be a viable option for the monitoring of the following issues in the RO system: extent of fouling and scaling, membrane compaction under high-pressure operations, and any mechanical leak involved in the RO element assembly that can affect the permeate flow rate. The NPF was attained by the following Equation (1).

$$Q_o \times ((P_i - \Delta P_i/2 - P_{pi} - \pi_i) \times TCF_i) / ((P_o - \Delta P_o/2 - P_{po} - \pi_o) \times TCF_o) = \text{Normalized flow rate } (Q_N) \quad (1)$$

where Q_o is measured (actual) permeate flow rate, P_i is initial operating pressure, P_o is actual operating pressure, ΔP_i is initial differential pressure, ΔP_o is actual differential pressure, P_{pi} is initial permeate pressure, P_{po} is actual permeate pressure, π_i is initial osmotic pressure derived from the logarithmic mean concentration of feed and concentrate, π_o is actual osmotic pressure derived from the logarithmic mean concentration of feed and concentrate, TCF_i is initial temperature correction factor, and TCF_o is actual temperature correction factor, respectively [23,39]. The term “initial” means the measured performance data at the initial point of RO system operation and the term “actual” implies the observed performance data at the certain point of time after starting RO system operation. RO membrane performance is largely affected by feed water temperature variations. Therefore, the temperature correction factor (TCF) must be considered to normalize the observed performance under varying temperature conditions to the temperature of initial system operation. The salt rejection (salt passage) is also a widely-used parameter for the monitoring of the RO system performance. Any operational or mechanical issues that arise in the RO system can be detected and revised beforehand through the monitoring of these performance parameters, prior to the occurrence of an irretrievable system performance deterioration. The NSP including the net driving pressure (NDP) can be derived by

the following equations (Equations (2) and (3)), and the normalized salt rejection (%) is also readily obtained by subtracting the NSP (%) from the integer 100.

$$\text{Normalized salt passage (\%)} = \frac{(C_{po} \times NDP_o \times TCF_i \times C_{fci} \times C_{fo})}{(C_{fco} \times NDP_i \times TCF_o \times C_{fco} \times C_{fi})} \quad (2)$$

where C_{po} is actual concentration of permeate, NDP_i is initial net driving pressure, NDP_o is actual net driving pressure, C_{fci} is initial logarithmic mean concentration of feed and concentrate, C_{fco} is actual logarithmic mean concentration of feed and concentrate, C_{fi} is initial concentration of feed, and C_{fo} is actual concentration of feed, respectively.

$$\text{Net driving pressure} = P - \Delta P/2 - P_p - \pi \quad (3)$$

where P is operating pressure, ΔP is differential pressure, P_p is permeate pressure, and π is osmotic pressure derived from the logarithmic mean concentration of feed and concentrate [7–9,19,23,39].

The feed water in the pilot test was fed into the two parallel pressure vessels of the pilot RO system after passing the conventional coagulation, sedimentation, and fine fibrous 5- μm microfilter filtration sequentially. The qualities of the feed and the permeate including the water temperature, silt density index (SDI), pH, and total dissolved solids (TDS) were monitored during the pilot test period. The individual ion concentration of the feed water was evaluated using ion chromatography (ICS3000 and DX500, Dionex), (Thermo Fisher Scientific, Waltham, MA, USA) and inductively coupled plasma optical emission spectrometry (Activa M, HORIBA Jobin Yvon S.A.S., Longjumeau, France). RO system simulation studies were conducted to estimate the average flux of the individual RO elements in a vessel, and the verification of the economic feasibility of LPRO was conducted using the RO system design software CSMPPro 5.0 that was provided by Toray Chemical Korea Inc. [39]. The input variables of RO system design software were adjusted based on the pilot-test results, and the predicted simulation results were considered in terms of the long-term system performance stability and the economic feasibility according to the flow rate of the adopted RO elements.

2.3. Laboratory Fouling Susceptibility Test

The fouling susceptibility values of both membranes (FLR, FEn) were evaluated prior to the actual long-term pilot test via a laboratory crossflow filtration system (Figure 2). Flat sheet coupons of both RO elements were kindly provided by Toray Chemical Korea Inc.

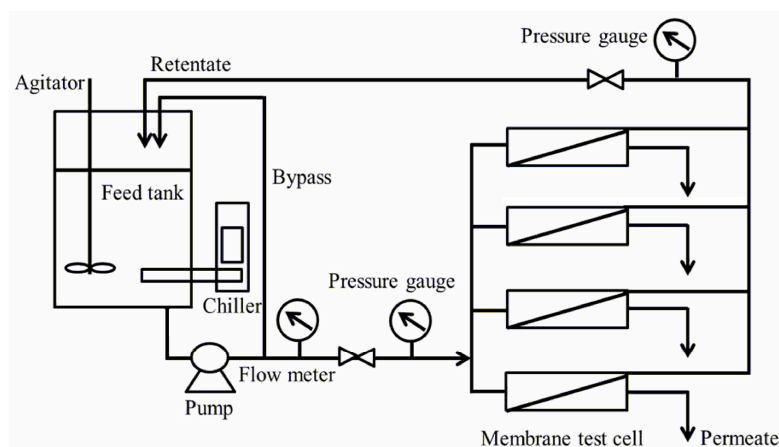


Figure 2. Schematic of flat sheet reverse osmosis crossflow filtration system.

Rectangular membrane samples with nominal dimensions of 7 cm \times 4 cm were placed in the membrane coupon test cells. The feed solution including 1500 ppm NaCl and individual model

foulants with a temperature of 25 °C and a pH of 7.0 was pumped from the feed tank and pressurized at 10.3 bar by a high-pressure pump at a flow rate of 1.0 gal/min (equivalent to 3.7854 L/min). The fouling susceptibility values of both membranes were estimated by measuring the flux decline ratio after a 2 h operation with the model foulant containing feed solution. The model foulants that were used for the organic, cationic, and anionic substances are 50 ppm dry milk, 5 ppm dodecyl trimethyl ammonium bromide (DTAB) (Sigma-Aldrich, St. Louis, MO, USA), and 50 ppm sodium dodecyl sulfate (SDS) (Sigma-Aldrich, St. Louis, MO, USA), respectively.

2.4. Membrane Analysis

The surface charge characteristics of the RO membranes expressed as streaming potentials were evaluated within the pH region of 4 to 10 through the use of a streaming potential analyzer (BI-EKA, Brookhaven, NY, USA) with a 1 mM KCl electrolyte solution. The surface features of the membranes were investigated with scanning electron microscopy (Novanano 230, FEI, Hillsboro, OR, USA) and atomic force microscopy (XE-150, PSIA, Lakewood, CO, USA). Contact angle measurements were conducted with a contact angle analyzer (VCA Optima, AST Products Inc., Billerica, MA, USA) through the application of the sessil drop method. ATR-FTIR (Nicolet 6700, Thermo Scientific, Waltham, MA, USA) spectrometer was used to evaluate the ratio of amide peak intensity (1540 cm^{-1}) to aromatic ring band intensity (1588 cm^{-1}).

Instrumental analyses on the membrane coupons and foulant samples obtained from the RO elements that were used for the pilot test were also carried out. The samplings of the fouled membranes and the accumulated foulants on the membrane surface were conducted at the lead position element of each pressure vessel. The surface morphology of the fouled membranes and the chemical element analysis of the foulant were performed using the scanning electron microscope (SEM) (Novanano 230) (FEI, Hillsboro, OR, USA) equipped with an energy dispersive X-ray spectroscopy (EDX) device (Apollo-XSDD) (EDAX, Mahwah, NJ, USA). The intensity of the organic fouling on each membrane was evaluated by measuring the total organic carbon (TOC) concentration. The fouled flat sheet membrane samples of 15 cm^2 that were extracted from the lead position elements were stored and agitated in 100 mL of deionized water at predetermined conditions (30 °C solution temperature, 7 days soaking time), and then the eluted organic content that had originated from the fouling layer on the membrane surface was analyzed by the TOC analyzer (TOC-500) (Shimadzu, Kyoto, Japan). The fractions of the organic and inorganic substances in the deposited foulant were determined according to the weight loss on ignition (LOI) method using the thermal gravimetric analysis (TGA). Generally, the weight LOI of the foulant was regarded as a practical indicative for the estimation of the occupying ratio of the organic and inorganic materials in the fouling layer. Gathered foulant samples from each RO element were gradually heated up to 700 °C using the TGA (Discovery) (TA Instruments, New Castle, DE, USA).

3. Results and Discussion

3.1. Laboratory Fouling Susceptibility Test and Pristine Membrane Analysis

Prior to conducting the long-term pilot test, the fouling susceptibility evaluations of both RO elements chosen in this study were carried out using the flat sheet membrane coupons at constant operating pressure mode. The base membrane performance described in Figure 3 is an average of four membrane coupons, and two of the four samples that are close to the average permeate flow rate were selected for the subsequent fouling resistance test.

The FLR exhibited a permeate flow rate that is almost 35% higher than that of the FEn with no noticeable difference in the salt rejection value. The FLR also showed a slightly higher flux decline ratio compared with the FEn for all of the fouling resistance tests using dry milk, DTAB, and SDS. An additional fouling resistance test for which the FEn permeate flow rate was adjusted up to that of the FLR was conducted to further verify the effect of the permeate flow rate on the membrane

fouling intensities [26,40–42]. The operating pressure was carefully increased to match the permeate flow rate of the FEn to the FLR level. The FEn flow-up case represented almost the same flux decline value compared with the FLR case. There was no significant difference in the fouling susceptibility between the FEn and FLR membranes, and this study shows that the anti-fouling characteristics of both membranes are almost analogous.

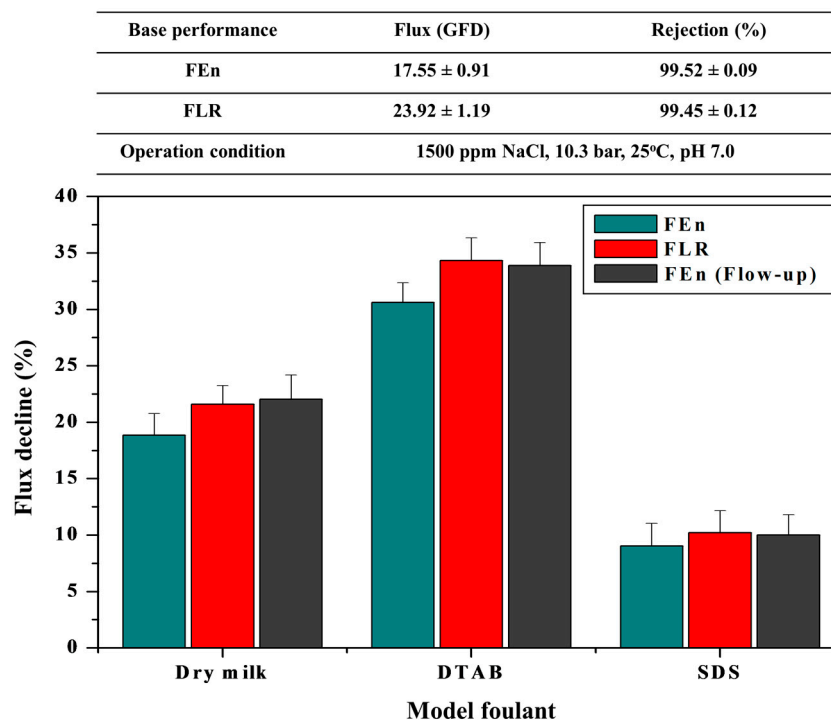


Figure 3. Flux decline comparison between the FEn and FLR adopting model foulants (Operation conditions: 1500 ppm NaCl, 10.3 bar, 25 °C, model foulants 50 ppm dry milk, 5 ppm DTAB, 50 ppm SDS, respectively).

The material composition and physical properties of FEn and FLR membranes were summarized in Table 2. Both membranes were typical thin film composite (TFC) aromatic polyamide RO membrane reinforced by the polysulfone support and polyester non-woven fabric. The ratio of amide peak intensity (1540 cm^{-1}) to aromatic ring band intensity (1588 cm^{-1}) of both membranes were estimated by FTIR analysis. The lower peak ratio of FLR membrane indicated that the LPRO membrane comprised relatively thinner polyamide active layer than that of FEn, which can be regarded as a primary reason for the higher flow rate of the LPRO FLR membrane. The FLR membrane coupon also exhibited a higher permeate flow rate than FEn.

Table 2. Details of the reverse osmosis membranes used in the experiments.

Name	Type	Material	IR Absorbance Ratio ($1540\text{ cm}^{-1}/1588\text{ cm}^{-1}$)	Flux (gfd ^a)	Rejection (%)	Test Conditions
FEn	TFC ^b	Aromatic polyamide	0.87	26.3	99.7	2000 ppm NaCl, 25 °C, 15.5 bar, pH 7
FLR			0.63	22.5	99.6	1500 ppm NaCl, 25 °C, 10.3 bar, pH 7

Notes: ^a gallon/ft²·day; ^b Thin film composite.

As shown in Figure 4, both membranes exhibited almost the same charge characteristics and hydrophilicity, irrespective of the membrane type. The surface structure was also investigated using SEM and atomic force microscope (AFM) (XE-150, PSIA). Typical ridges and valleys on the surface structure of the polyamide-based RO membrane could be confirmed for both membranes from the SEM images (Figure 5), and there is no notable difference between the two membranes.

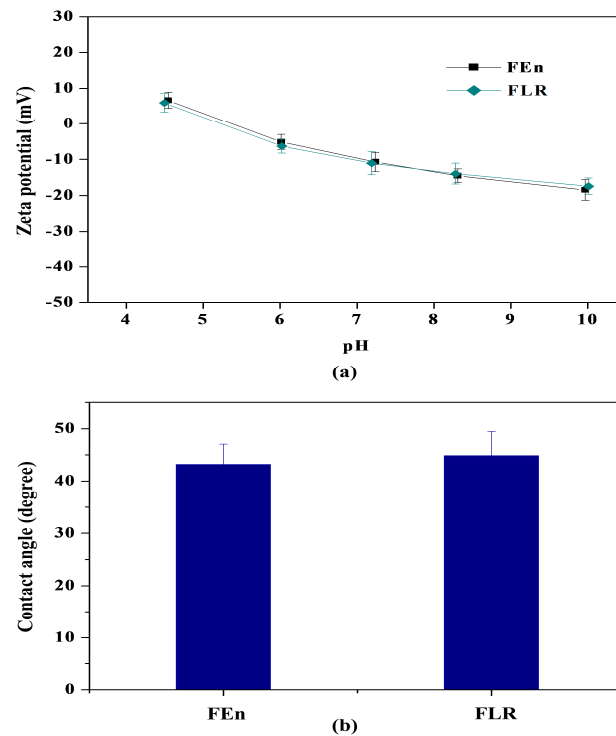


Figure 4. Comparison of surface characteristics of the membranes with different flow rates: (a) Zeta potential; (b) Sessile drop contact angle.

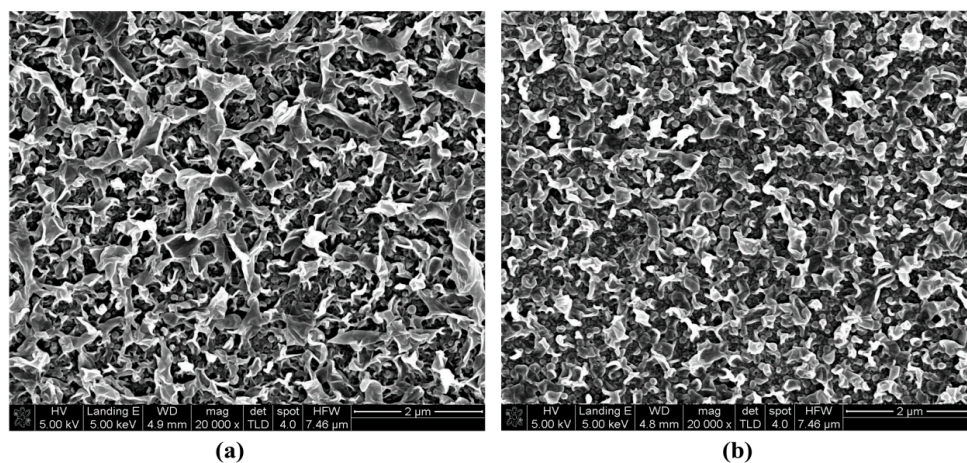


Figure 5. SEM images of the neat membranes: (a) FEn; (b) FLR ($\times 20,000$).

The surface morphology analysis results from the AFM also showed a comparable trend. The definitions of projected area and mean height are defined as the product of x and y range in the selected area scanned by AFM and the average height of the height profiles within the area, respectively. As described in Table 3, both the root mean square roughness (R_{ms}) and the peak-to-valley (R_{p-v}) distance of the two membranes did not reveal major differences. To summarize, both the FEn and FLR

membranes exhibited quite similar surface characteristics, such as the structural morphology, surface charge, hydrophilicity, and fouling resistance, with the permeate flow rate being the only exception.

Table 3. Root mean square roughness (R_{ms}) and peak to valley distance (R_{p-v}) of FEn and FLR membranes, as observed via AFM.

Sample	R_{p-v} (nm)	R_{ms} (nm)	Mean Height (nm)	Projected Area (μm^2)
FEn	585.8	69.93	249.3	25
FLR	568.2	63.39	176.1	25

3.2. Operating-Pressure Variations According to the Permeate Flow Rate of the RO Elements

A pilot RO system was operated at constant flow rate mode, and the qualities of water solution used in the pilot test are described in Table 4. Considering the general guidelines for the RO feed water qualities, the TOC, SDI, and turbidity values of the raw water are over the maximum allowable ranges [7,8,39]. After a 646 h operation, the retentate of each vessel was recycled to the feed water to generate a higher-fouling-potential feed water condition (Figure 1), and as shown in Table 4, the TOC, SDI, and turbidity noticeably increased after the recycling of the retentate.

Table 4. Description of feed water quality and operation condition.

Operation Variables and Ion Species			Start~646 h	646~872 h	Features
Operation Condition	Permeate (m^3/h)		$2.2 \text{ m}^3/\text{h}$	$2.2 \text{ m}^3/\text{h}$	Retentate recycle (646 h~)
	Recovery (%)		33%	85%	
Water Quality	Al	mg/L	0.12	0.19	
	Si	mg/L	2.3	2.9	
	Mn	mg/L	N.D ^a	N.D ^a	
	B	mg/L	0.06	0.11	
	Ba	mg/L	N.D ^a	0.05	
	Sr	mg/L	N.D ^a	N.D ^a	
	Na^+	mg/L	89.0	119.6	
	K^+	mg/L	12.0	13.8	
	Mg^{2+}	mg/L	12.0	14.5	
	Ca^{2+}	mg/L	72.1	94.7	
	Cl^-	mg/L	107.3	140.2	
	NO_3^-	mg/L	19.7	23.6	
	SO_4^{2-}	mg/L	145.6	193.0	
	pH	-	7.0	7.3	
	Conductivity	$\mu\text{S}/\text{cm}$	894.6	1141.7	
	TOC	mg/L	3.5	4.6	
SDI	-	5.2	6.3		
Turbidity	NTU	0.3	0.5		

Note: ^a Not detectable.

The total operation period (872 h) was segmented by a three-operation period on the basis of the cleaning in place (CIP) intervals. Initially, the CIP was to be conducted when the differential pressure of each vessel reached 1 bar; however, the CIP was performed simultaneously at the two pressure vessels due to the almost similar differential pressure build-up trend of both vessels. Detailed CIP sequences are described in Table 5, and the CIP protocol was optimized via the preliminary pilot test study and the operational experience of the main RO plant, which was treated the same feed water as the pilot RO system [18].

Table 5. CIP procedure applied in this study.

CIP Procedure of Pilot RO System
1. Preparing inorganic cleaning solution ^a : 1% cleaning chemical, pH 2.5, 35 °C
2. Recycling for 1 h with inorganic cleaning solution at 2 bar, flow rate 6 m ³ /h
3. Soaking for additional 16 h with inorganic cleaning solution and flush the system
4. Preparing organic cleaning solution ^b : 1% cleaning chemical, pH 10.5, 35 °C
5. Recycling for 1 h with organic cleaning solution at 2 bar, flow rate 6 m ³ /h
6. Soaking for additional 1 h with organic cleaning solution
7. Recycling for 1 h with organic cleaning solution at 2 bar, flow rate 6 m ³ /h
8. Soaking for additional 1 h with organic cleaning solution
9. Flush the system and then start the normal operation

Notes: ^a Inorganic cleaning agent (Purichem MC-128K, Primetech International Co., Ltd., Gyeonggi-Do, Korea);

^b Organic cleaning agent (Purichem MC-254K, Primetech International Co., Ltd., Gyeonggi-Do, Korea).

At first, the operating pressure variation trend was monitored. The raw water qualities including the TOC, SDI, and turbidity were not suitable for the stable RO operation, so the membrane fouling propensity was inevitably high. Consequently, as shown in Figure 6a, both vessels exhibited gradually increasing operating pressure trends with increasing operation time. As a result, the first CIP point emerged after approximately 450 h of operation, while about 200 h of operation was enough to reach the additional designated CIP point. Interestingly, while the FEn vessel exhibited the decreased operating pressure value below its initial value, a slightly increased operating pressure was confirmed in the FLR vessel after the conduction of the first CIP. Considering the same CIP condition for both vessels, it could be concluded that the membrane fouling is relatively severe (less cleaning efficiency) in the FLR vessel.

The accumulative membrane fouling along with the increased operation time surely decreased the CIP interval, and the intensity of the membrane fouling, which can be expressed as an increase in the operating pressure, is considerably higher in the third operation period compared with the other operation periods due to the enhanced fouling potential condition of the third period. The operating-pressure drop that occurred at the second operation period start-up point of the FEn vessel and at the third operation period start-up point (Figure 6a) of both vessels is mainly attributed to the feed water temperature increase that was led by the retentate recycling and the CIP induced swelling effect. The average feed water temperature during the first and second operation periods is 23.2 °C, but this increased to 26.6 °C during the third operation period due to the retentate recycling. According to the RO membrane temperature correction factor, an about 4% increase of the permeate flow rate was obtained per 1 °C increase of the feed water temperature [7,8,39]. As described in Table 5, the CIP protocol in this study repeated the acid and base condition cleanings in a sequential manner. The polyamide membrane is known to be swollen at the base condition due to the deprotonation of the carboxylic acid groups within membrane structure [43,44]. The swelling of the polyamide led to more permeable membrane structure, causing lowered operating pressures.

The data abnormality that occurred in the FLR vessel at around the 800 h mark in the third operation period is due to a mechanical issue in the pilot system (Figure 6a). At that time, the automatic valve equipped in the permeate stream of the FLR array malfunctioned, so the actual permeate flow decreased to less than 1.9 ton/h and the operating pressure was also maintained relatively low. After the repair of the automatic valve, the performance indicatives of the FLR vessel, including the flow rate and the operating pressure, recovered to the initially designed value. To validate the performance variation between the two vessels, the operating pressure increasing tendency of each operation period was estimated by comparing the operating pressures of the start-up point and end-point of each operation period. The operating pressure increment was attained by the following Equation (4).

$$\text{Operating-pressure increment (\%)} = 100 \times ((P_e - P_i) / P_e) \tag{4}$$

where P_e is operating pressure at the end-point of each period, and P_i is operating pressure at the initial point of each period, respectively.

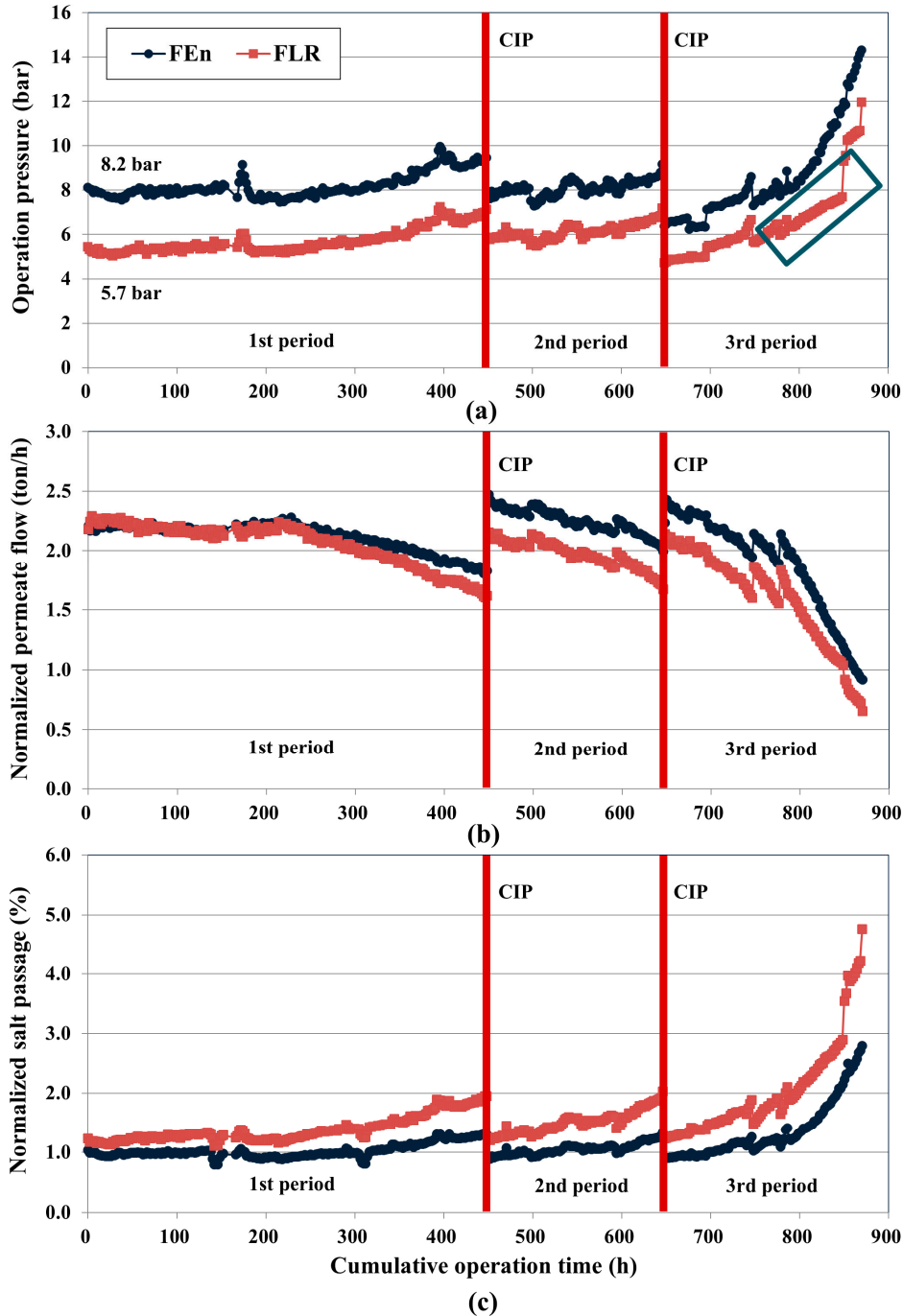


Figure 6. Performance variations monitoring of the pilot RO system: (a) Operating pressure variations of the FEn and FLR; (b) Normalized permeate flow (NPF) variations of the FEn and FLR; (c) Normalized salt passage (NSP) variations of the FEn and FLR.

As can be seen in Figure 7, both vessels exhibited an increased operating pressure with increasing operation time, which inferred the occurrence of the accumulative membrane fouling. In addition, the FLR vessel showed a pronounced operating pressure increasing tendency throughout the test

period, suggesting a more intensified fouling in the FLR vessel. Especially, during the third period of operation for which retentate recycling was adopted to generate higher fouling potential feed water condition, the highest operating pressure increasing tendency was confirmed for both vessels. The operating pressure gap ratio between the two vessels was also evaluated using the following Equation (5).

$$\text{Operating pressure difference ratio (\%)} = 100 \times ((P_{\text{FEn}}/P_{\text{FLR}}) - 1) \quad (5)$$

where P_{FEn} is operating pressure of FEn and P_{FLR} is operating pressure of FLR, respectively. As can be seen in Figure 6a, the feed pressures at the initial point of operation are 8.2 bar for the FEn vessel and 5.7 bar for the FLR vessel. The initial operating pressure difference clearly originated from the inherent flow rate difference of both RO elements. However, as can be seen in Figure 8, the operating pressure difference ratio between the two vessels became smaller as the cumulative operation time was increased. At the initial stage of operation, a roughly-50%-higher operating pressure was needed for the FEn vessel to meet the designed permeate flow rate 2.2 ton/h, but the pressure difference gap ratio decreased to approximately 32% during the first period of operation (start-up to 448 h). The CIP conducted at the end of the first period could not recover the initial pressure difference ratio between the two vessels, and the decreased pressure difference ratio was almost maintained during the remaining operation period (448 h to 872 h); this is mainly due to the fact that the FLR vessel exhibited a higher operating pressure increasing tendency compared with the FEn vessel. The fluctuation of the operating pressure difference ratio during the third operation period was caused by the previously described permeate stream autovalve error of the FLR installed RO array. Noticeably, the least pressure difference was estimated at the end-point of the third operation period, which could be considered as the most severe fouling occurrence condition. As previously described, the retentate of each vessel was recycled to generate the higher fouling potential condition during the third period of operation. This result suggests that the advantage of a low-pressure RO membrane, which could lower the operating pressure, can be diminished at the high fouling potential operation condition.

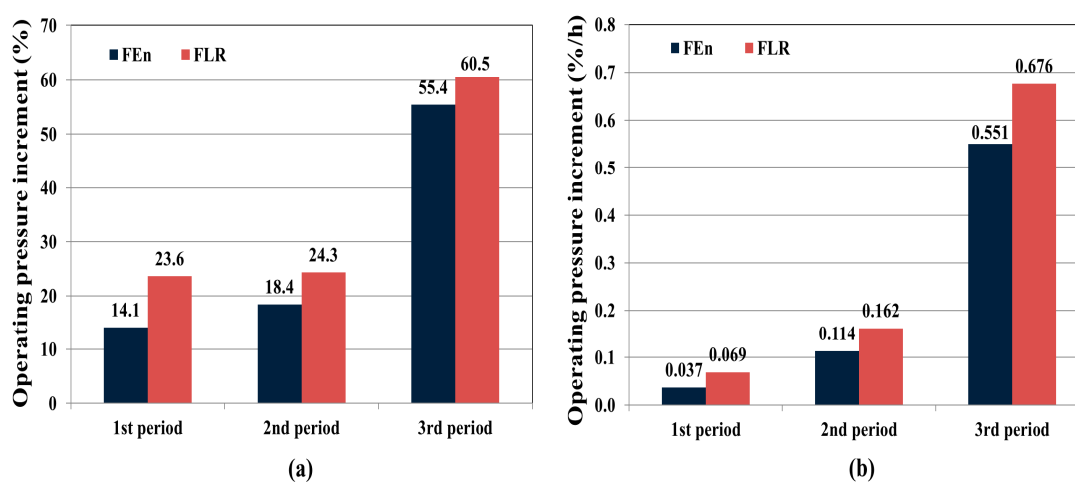


Figure 7. Operating pressure increment comparison between the FEn and FLR based on the segmented operation period: (a) Operating pressure increment (%) between initial start-up and end-point of each periods; (b) Operating pressure increasing rate (%/h) of each periods.

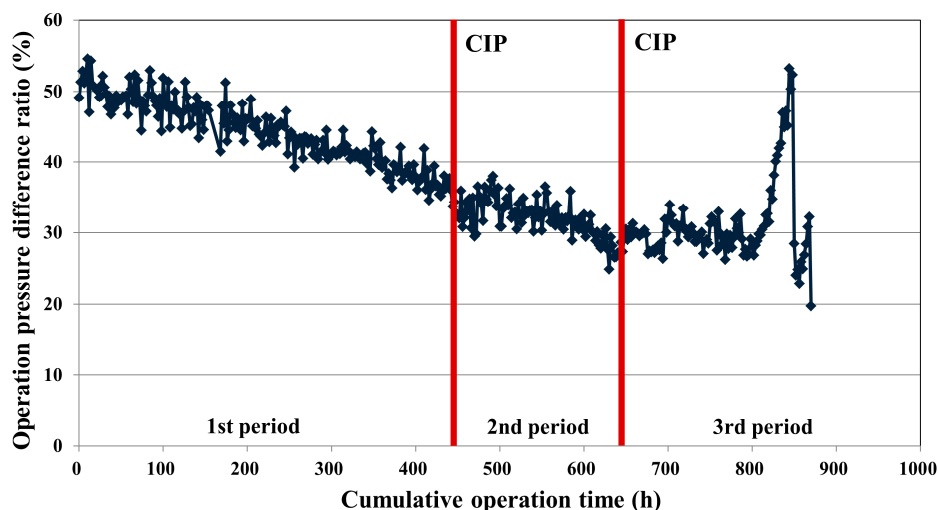


Figure 8. Operating pressure difference ratio between the FEn and FLR according to the cumulative operation time.

3.3. Variations of the Normalized Permeate Flow Rate (NPF) and Normalized Salt Passage (NSP) According to the Permeate Flow Rate of the RO Elements

The normalization of flow rate and salt passage was conducted to determine the noticeable variations in the system performance that originated from the membrane fouling. The NPF of both vessels was maintained constantly without a noticeable change until 200 h of operation (Figure 6b), but a gradual decreasing tendency was confirmed after 200 h operation. The FLR adopted vessel exhibited a larger NPF decline compared with the FEn during the first operation period. Similar to the operating pressure variation case, the FEn vessel showed increased NPF values at the start-up points of the second and third periods due to the CIP induced swelling effect. The NPF difference between the two vessels at the start-up point of the second operation period is more enhanced after the conduction of the CIP, which suggests that a more intensive fouling (less cleaning efficiency) occurred in the FLR vessel during the first operation period; and this trend is similar to the operating pressure drop confirmed in Section 3.2. Compared to the operating pressure variation depicted in Figure 6a, however, the NPF variation is much more relieved in the third period of operation, because the NPF calculation accounted for the flow rate variation that was induced by the water temperature fluctuation.

The permeate flow variation rate (PVR, ton/h) was estimated according to the segmented operation terms. The permeate flow variation rate was calculated on the basis of time rate of change in NPF between the start-up point and end-point during the operation. As described in Table 6, both vessels exhibited negative PVR values which inferred the decrease of the NPF, and the FLR showed a larger PVR decline compared with the FEn during the entire test period. Specifically, the FLR exhibited an approximately 50% higher PVR decrease value compared with the FEn during the first operation period, which can be regarded as similar to the trend that was observed in the operating pressure study. Furthermore, the PVR decline values of both vessels became larger as the cumulative operation time was increased. Noticeably, the NPF and PVR remarkably decreased during the third operation period for which the high fouling potential operation condition was adopted. The increase of the cumulative operating time and the high fouling potential condition in the third operation period can lead to the intensive membrane fouling, and the degree of membrane fouling that was expressed as the decreased NPF and enhanced PVR-decline values is more pronounced for the FLR case.

Table 6. Permeate flow variation rate (PVR) and salt passage variation rate (SVR) of both membranes according to the segmented operation periods.

Performance Monitoring Parameters	Sample	1st Operation Period	2nd Operation Period	3rd Operation Period	Entire Test Period
Permeate flow variation rate (PVR, ton/h) ^a	FEn	−0.00086	−0.00232	−0.00583	−0.00148
	FLR	−0.00125	−0.00243	−0.00657	−0.00175
Salt passage variation rate (SVR, %/h) ^b	FEn	0.00060	0.00220	0.00836	0.00201
	FLR	0.00162	0.00418	0.01562	0.00405

Notes: ^a Permeate flow variation rate = (NPF difference between start-up and end point of given operation period)/(elapsed operation time of given operation period); ^b Salt passage variation rate = (NSP difference between start-up and end point of given operation period)/(elapsed operation time of given operation period).

Apparently, the NSP provided a more distinctive performance deterioration behavior in the FLR case (Figure 6c). FLR vessel showed a slightly higher salt passage due to the lower operating pressure compared with that of the FEn at the initial operation stage. However, the NSP difference between the two vessels became larger even though the FLR vessel experienced a higher operating pressure increasing tendency compared with the FEn during the entire operation period. The NSP of both vessels almost recovered to the initial values after the conduction of CIP, but a more rapid NSP increasing behavior was confirmed in the subsequent plant operation. Contrary to the operating pressure and NPF variation trends, the NSP difference between the two vessels started to become larger just after the initial operation start-up point. The salt passage variation rate (SVR, %/h) was also evaluated (Table 6). Similar to the PVR, the SVR can be estimated from the NSP difference and the elapsed operation time of the given operation period. Compared with the FEn vessel, the SVR increase of the FLR vessel is approximately 2.5 times higher during the first operation period, and then an approximately twofold increase of the SVR was maintained during the remaining operation period, showing more accumulation of fouling and subsequent rejection decline in FLR.

Figure 9 describes the simulation study results for the average permeate flux of the individual elements in a pressure vessel using RO system design software CSMPro 5.0. The flux variation behaviors of the FEn and FLR were compared according to the element position in a vessel. Both cases showed the highest average flux for the lead position element and the lowest average flux for the end position element. Considering the increased feed water concentration and the NDP decline that were caused by the filtered water through the fore positioned elements, the lowest flux of the end position element is quite reasonable. Notably, the FLR case exhibited the larger average flux difference between the lead and end position elements compared with the FEn. The localized working load within a pressure vessel that is due to an uneven individual element average flux may accelerate the fouling of the lead position element, which could lead to an enhanced salt passage. The membrane fouling propensity increased with the operational flux. Consequently, the higher flow rate operation of the lead position element of the FLR vessel caused a more intensified membrane fouling. Alternatively, the FEn adopted case may generate a more even working load distribution within a vessel, which enables a more stable system operation.

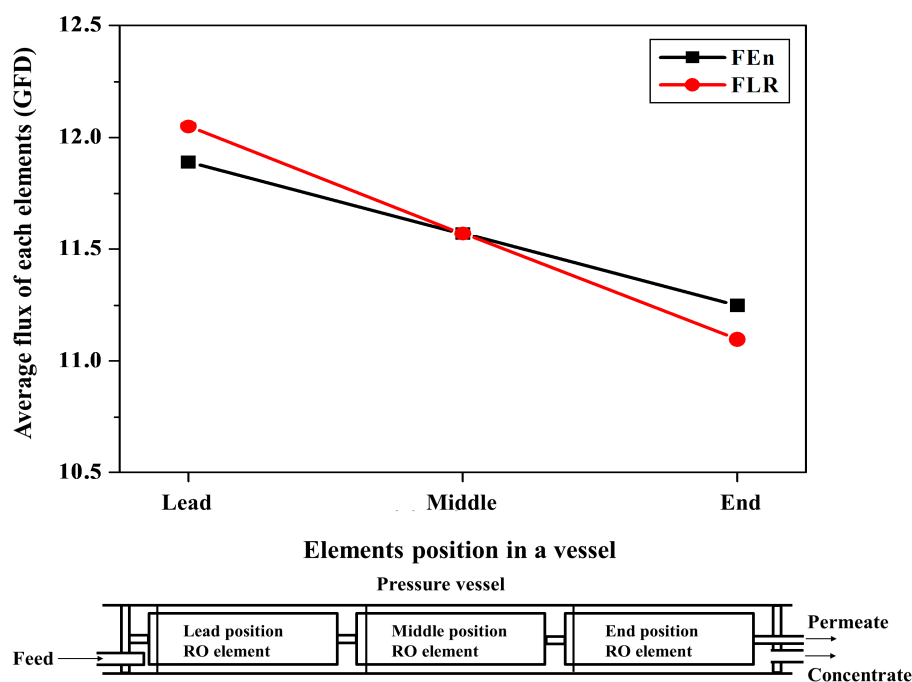


Figure 9. Predicted average flux of the individual elements from the simulation study according to the located position in a vessel and permeate flow rate of RO elements.

3.4. Estimation of Individual Element Performances

The individual element performances including the permeate flow, salt rejection, and differential pressure were estimated. The differential pressure is the difference between the feed pressure and the brine pressure existing at the end of the elements. Therefore, the differential pressure of the individual RO elements can be obtained by measuring the pressure drop as the feed water passes through the feed channels. The feed channel blocking that is due to the membrane fouling can lead an increase in the differential pressure, which can be an indicative of the estimation of the fouling intensity of each RO element. The differential pressure of the pilot RO system was also measured during the pilot test; however, due to the relatively short test term, the differential pressure gap between pressure vessels is not perceptible. Instead, the differential pressure of the individual RO elements before and after the pilot test was measured to compare the fouling intensities according to the element flow rate. A total of six RO elements were uninstalled from the pilot test machine after finishing the test and then sent to the Toray Chemical Korea Inc. plant to assess the element performance including the differential pressure. The performance deterioration values of the used RO elements were estimated through a comparison of the retest results to those of the initial performance that were measured prior to the pilot test. Specifically, the performance variation according to the RO element flow rate was evaluated by comparing the membrane performances of the corresponding position RO elements between the two vessels [18]. The element performance was evaluated based on the regular grade RO (FEn) standard test condition at 2000 ppm NaCl, 25 °C, 15% recovery, 15.5 bar, and pH 7.0.

As described in Figure 10, the lead position FLR element showed an enhanced flow rate decrease and salt passage increase compared with the FEn located at the same position in a vessel. The end position FLR element exhibited a rather lower flow rate reduction compared with the FEn. In particular, even though the overall differential pressure that was measured during the pilot test is superficially analogous for both vessels, the differential pressure deviation of the individual elements within the same vessel is more prominent in the FLR case compared with the FEn case, which further confirmed that the membrane fouling of the lead position element is more pronounced in the FLR case. Accordingly, the FLR case also showed a larger differential pressure gap between the lead and end

position elements. As can be seen in Figure 10, the differential pressure gaps within a vessel are 0.08 bar for the FEn case and 0.20 bar for the FLR case. In conclusion, the performance deterioration, including the flux decline, salt passage increase, and differential pressure increase is more enhanced and localized on the lead position element and the intensity is considerably higher in the FLR case compared with the FEn case; this is mainly due to the fact that the lead position FLR element experienced an enhanced working load due to its inherent higher permeability.

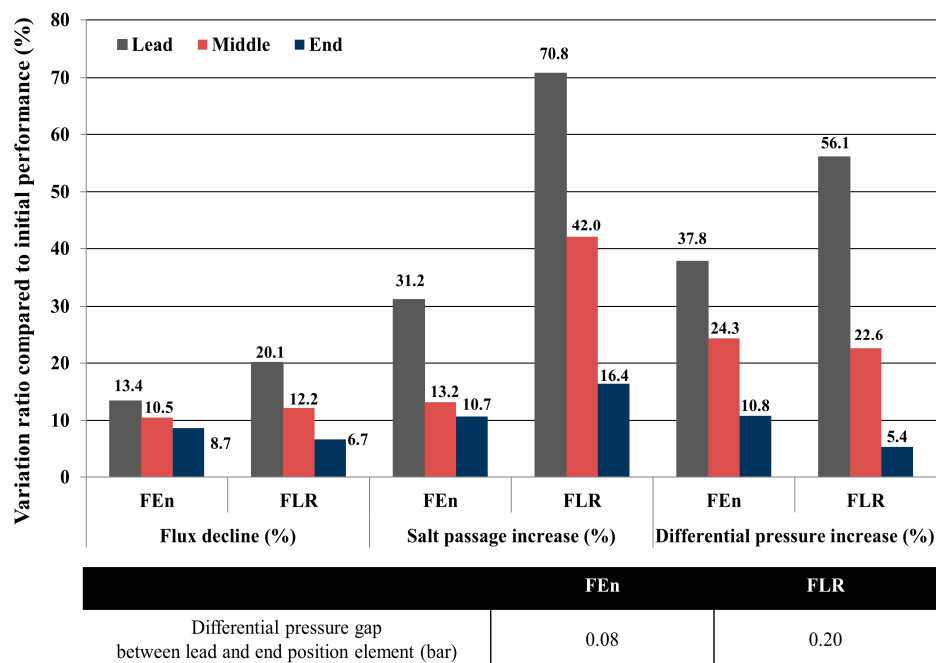


Figure 10. Comparison of the individual element flux decline, salt passage increase, and differential pressure variation according to the installed position in a vessel.

3.5. Membrane and Foulant Analysis

The lead position elements of both vessels were further inspected with diverse analytic methods. It was known that different types of foulants and scalants were characterized in each RO elements according to its specific position within a pressure vessel [45,46]. Each RO element was autopsied for the extraction of the flat sheet membrane samples and the foulants accumulated on the membrane surfaces. At first, the surface features of the virgin and fouled membranes were visualized. As shown in Figure 11, when the SEM images of fouled membranes were compared with different flow rates, the fouling layer magnitude of the FLR case appears to be quite different compared with the FEn case. Considering the fact that the two elements were operated under parallel operational conditions, including the feed water characteristics, and had a correlative intrinsic fouling resistance, as described in Section 3.1, the differences in the fouling layer details are principally due to the more intensive fouling of the FLR that originated from its intrinsic higher flow rate.

The organic and inorganic occupying portions of the foulant were evaluated using weight LOI method. By adopting the LOI method, the organic substance fraction in the foulant samples can be estimated through a measurement of the weight variation after the heating of the samples to the previously designed temperature. Generally, the remaining water in the prepared foulant samples vaporized at temperatures below 100 °C. As a result, the organic/inorganic fractions of foulants can be determined by measuring the weight variation between the weights of around 105 °C and the final temperature. As shown in Figure 12, an approximate weight loss of 40% was estimated, indicating that the volatile organic materials occupied a 40% fraction of the foulant, and approximately 60% of the remaining weight originated from inorganic materials, irrespective of the RO element permeate

flow rate. These results indicate that the organic/inorganic portion of foulants remains as analogous even though the fouling intensities in the two foulant samples are different.

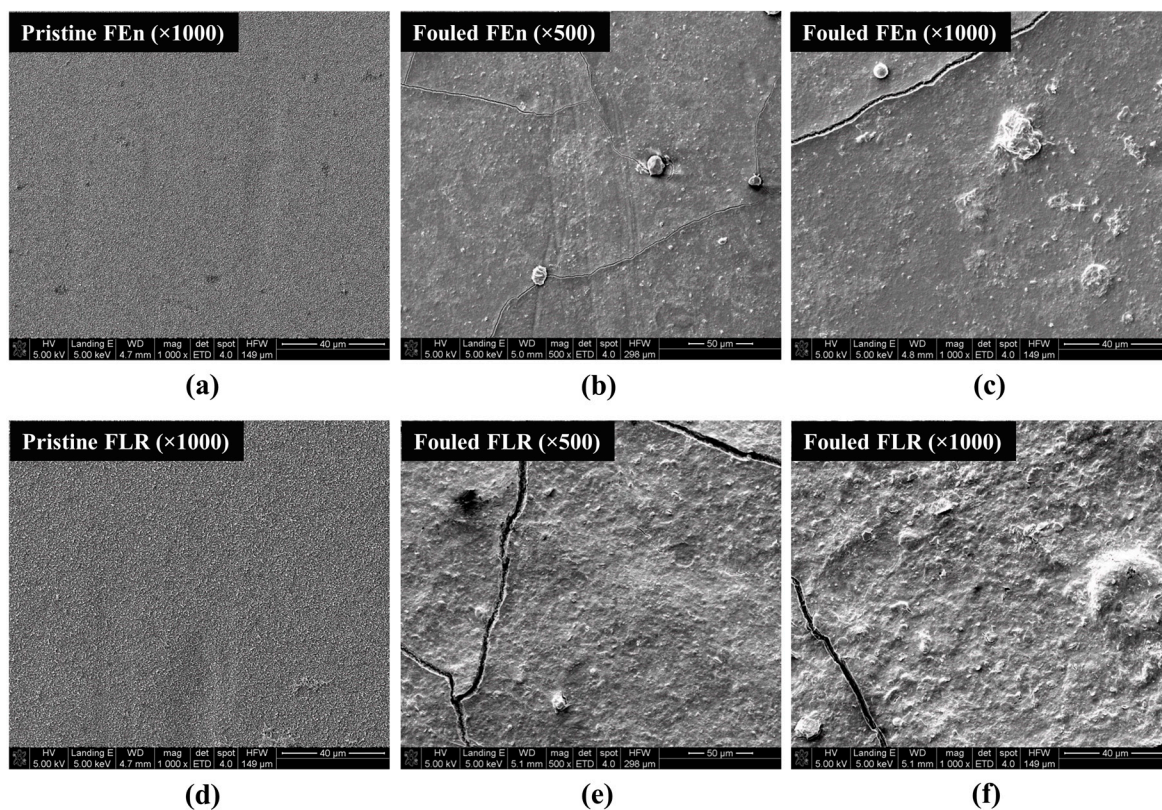


Figure 11. SEM images of the fouled and pristine membranes: (a) Pristine FEn ($\times 1000$); (b) Fouled FEn ($\times 500$); (c) Fouled FEn ($\times 1000$); (d) Pristine FLR ($\times 1000$); (e) Fouled FLR ($\times 500$); (f) Fouled FLR ($\times 1000$).

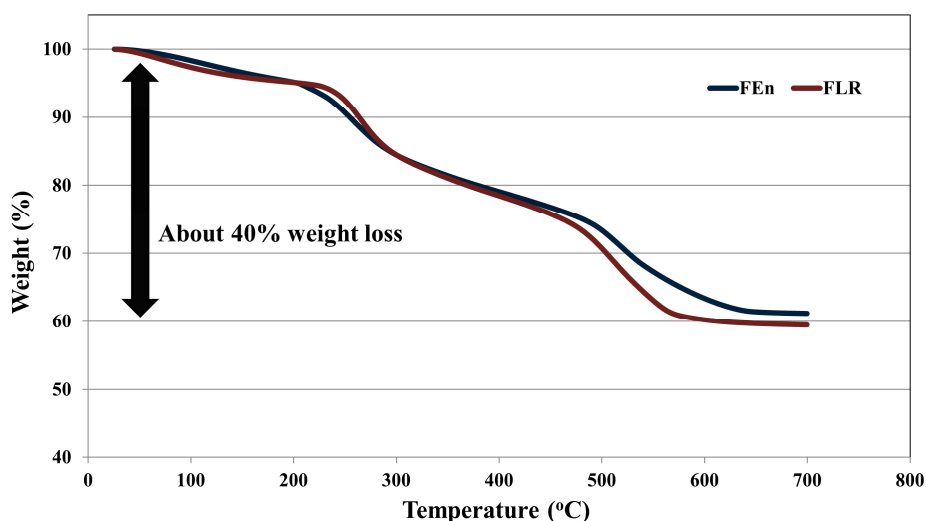


Figure 12. Thermal gravimetric analysis (TGA) curves of the foulant samples acquired from the lead position FEn and FLR elements.

The EDX analysis was conducted to determine the elemental composition of the foulants on the membrane surfaces. EDX can also be adopted as an indirect analytic tool for estimating the foulant

amount due to an energy intensity that is comparative to the element concentration. According to Figure 13, both the chemical composition and the peak intensities appear to be similar and are not dependent on the RO element flow rate grade. Notably, the inorganic fouling sources mainly consist of aluminum and silica. There was a slight possibility of an exclusive silica deposition on the membrane surface, because silica exists in most water sources abundantly, and the feed water silica concentration was managed within the region of 2.3 ppm to 2.9 ppm during the test period. Aluminum, however, is known as one of the most dominant precipitants, and the aluminum concentration is noticeably higher than the RO feed water guideline of 0.05 ppm [39]. As described in Table 4, the aluminum concentration varied from the initial value of 0.12 ppm to 0.19 ppm after the retentate recycling, and this value is almost two-to-four times higher than the guideline limitation. Consequently, the aluminum and silica formed insoluble aluminum-silicate deposits on the membrane surface [18].

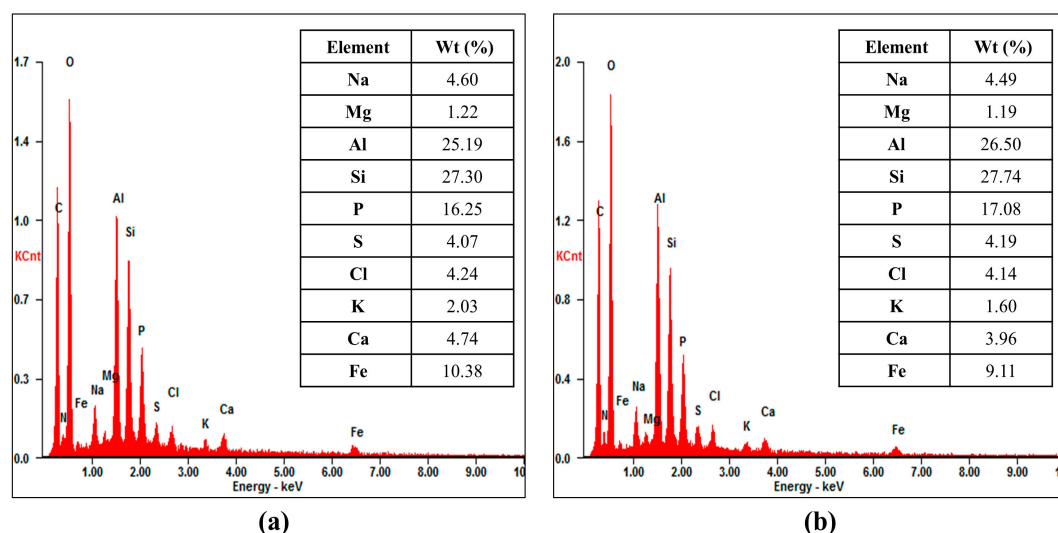


Figure 13. EDX chemical precipitations on the fouled RO membrane: (a) FEn; (b) FLR.

The TOC measurements of the eluted organic materials from the fouled membranes were conducted to quantitatively compare the organic fouling intensity of the two membranes (Figure 14). Fouled flat sheet membrane samples of 15 cm², which were extracted from the lead position elements of both vessels, were stored and agitated in 100 mL of deionized water at predetermined conditions (30 °C solution temperature, 7 days soaking time), and then the eluted organic content was filtered with a 0.45 μm prefilter before it was subjected to the TOC analyzer. The averaged value of the six experimental TOC analysis runs was calculated. The FLR case showed a higher eluted organic substance concentration than the FEn case. It could, therefore, be concluded that the LPRO operation treating the high fouling potential feed water evidently increased the fouling propensity to the organic foulants. Notably, the pristine membrane sample that was adopted as a reference also exhibited low organic concentration levels; this seems to be due to the trace of the residual chemicals that were applied for the polysulfone support and the polyamide thin layer formation in the RO membrane preparation process. However, these residual chemicals should be thoroughly washed out during the RO element performance measurement and flushing processes.

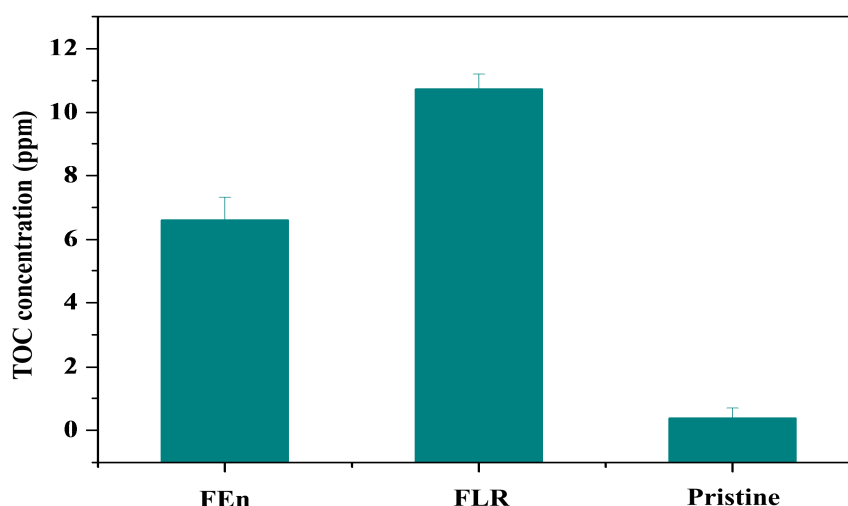


Figure 14. Total organic carbon (TOC) concentration of the eluted organics from the foulants on the membrane surface.

3.6. LPRO Feasibility Estimation Study Based on the Pilot Test Results

The economic and practical feasibility of LPRO was evaluated through the simulation study using RO system design software CSMPPro 5.0 (Toray Chemical Korea Inc.). It was assumed that a reuse plant with a 50,000 ton/day capacity was designed with the adoption of either the FEn or the FLR, and the other design details are shown in the Table 7. As shown in Table 7, the same numbers of pressure vessels and RO elements were derived, so there would be no difference in the capital cost for both simulation cases. The operation cost difference between the two simulation cases could be estimated by comparing the specific energy consumption (kWh/ton) that is calculated from the predicted operating pressure. On the other hand, the allowable minimum salt rejection value of the system was presumed as 98% to estimate the effect of the different flow rate RO elements on the permeate water quality. Other design details such as the array configuration, system recovery, and average permeate flux, were determined according to the conventional reuse plant design protocol provided by the filter technical support team of Toray Chemical Korea Inc.

Table 7. Design parameters for the simulation study to estimate the LPRO feasibility.

Design Parameter	Details
Designated product flow	50,000 ton/day
Membrane type and model	Case 1: RE8040-FEn, Case 2: RE8040-FLR
Array configuration	2 Array (270: 1st stage, 135: 2nd stage), 6 Elements/pressure vessel
Recovery ratio (%)	75%
No. of pressure vessel (EA)	405
No. of element (EA)	2430
Average permeate flux (GFD)	13.6

The annual flux decline value (%/year) and the annual salt passage increase value (%/year) were adjusted based on the preceding pilot test result. According to Table 6, the FLR case represented a permeate flux decline tendency that was enhanced by roughly 20% during the entire operation period, so the annual flux decline of the FLR case was adjusted as 14.4%/year, which is a 20%-higher value compared with the default setting of 12%/year that is commonly applied for the reuse plant design process. Accordingly, the 12%/year annual flux decline setting was adopted for the FEn case for the simulation study. The annual salt passage increase (%/year) value of the FLR was also adjusted because the FLR exhibited a salt passage increasing tendency that is almost twice as high during

the entire pilot test period. The annual salt passage increase settings of both cases were assumed as the default value of 10%/year for the FEn case, which is normally adopted for the reuse plant design process, and 20%/year for the FLR case. These default setting values are exactly same as those of RO design software IMSDesign 2015 (Hydranautics, Oceanside, CA, USA). On the other hand, other design programs including DS2 (Toray Industries Inc., Tokyo, Japan) and ROSA (Dow Chemical Company, Midland, MI, USA) set the default setting values slightly conservative compared to those of CSMPPro 5.0 and IMSDesign 2015. The setting values of each RO membrane manufacturer were derived from the internal test results and the empirical field data acquired from various applications [47–50]. An additional FLR based simulation study for which the default values of both the annual flux decline and the annual salt passage increase were adopted was also conducted to estimate the effect of the adjusted input variables on the simulation results.

Figure 15a shows the annual specific energy consumption (kWh/ton) estimation result of the simulation studies. The specific energy consumption (operating pressure) of FEn case was 22.5% higher than those of FLR cases at the beginning of the system operation (0 year). When comparing the FEn and the 12%/year annual flux decline FLR case, the difference in the operating pressure (expressed as specific energy consumption) was predicted to increase from 22.5% (0 year) to 27.0% (5 year) as the operation year elapsed. Consequently, the average operating difference ratio was calculated as 24.4% during entire operation period (5 years). On the other hand, an additional FLR based simulation study for which adopting the annual flux decline setting as 14.4%/year exhibited considerably different variations. In this case, the operating pressure difference ratio was expected to decrease from 22.5% (0 year) to 14.3% (5 year) as the operation time elapsed, and the average operating pressure difference ratio was calculated as 17.8% during the same operation period. As a result, it could be confirmed that the energy saving advantage of the LPRO application could be significantly reduced in the long-term operation. Although it was predicted that the FLR was fairly advantageous for lowering the operating pressure at the initial stage of system operation, it was necessary to make a comprehensive judgment with considering the enhanced flux decline accompanied by the frequent CIP intervals and the following product water quality issue.

As shown in Figure 15b, the system rejection prediction results addressed another serious issue in the model plant management. As previously described, a 98% system rejection was presumed as the minimum allowable value for the permeate water quality. For the FEn case, it was predicted that the permeate water quality could meet the designated water criteria up to the fifth year without an RO element replacement; however, the system rejection of the FLR case was predicted as 97.7% at the second year for the 20%/year salt passage increase case and 97.8% at the third year for the 10%/year salt passage increase case. This is mainly due to the lower operating pressure and the higher annual salt passage increasing tendency of the FLR. The required quantity of the FLR elements to meet the presumed system rejection of 98% can be estimated by varying the partial replacement ratio. As can be seen in Table 8, 83.3% of the total FLR elements must be replaced at the second year for the 20%/year annual salt passage case, and a 50% element replacement is needed at the third year for the 10%/year annual salt passage case. The term “element average age” in Table 8, means the maximum allowable element average age to match the desired permeate water quality. That is, a significant amount of FLR elements must be partially replaced in the subsequent operation year to maintain the required element average age and the consequent permeate water quality.

When considering the inevitable element replacement cost, including the RO element purchase, labor cost, auxiliary devices cost, and the plant shutdown loss during the RO element replacement, the operating cost saving obtained from the lowering of the operating pressure could be offset eventually in the long-term operation. To summarize, LPRO exhibited a higher salt passage increase and an enhanced permeate flow rate decrease when it was facing the high fouling potential feed water. So, to utilize LPRO stably during long-term commercial operations, a highly advanced pretreatment process installation must occur first. Therefore, the LPRO application for high fouling potential

feed water must be determined with careful consideration in terms of the initial capital cost and the operation and maintenance (O&M) cost.

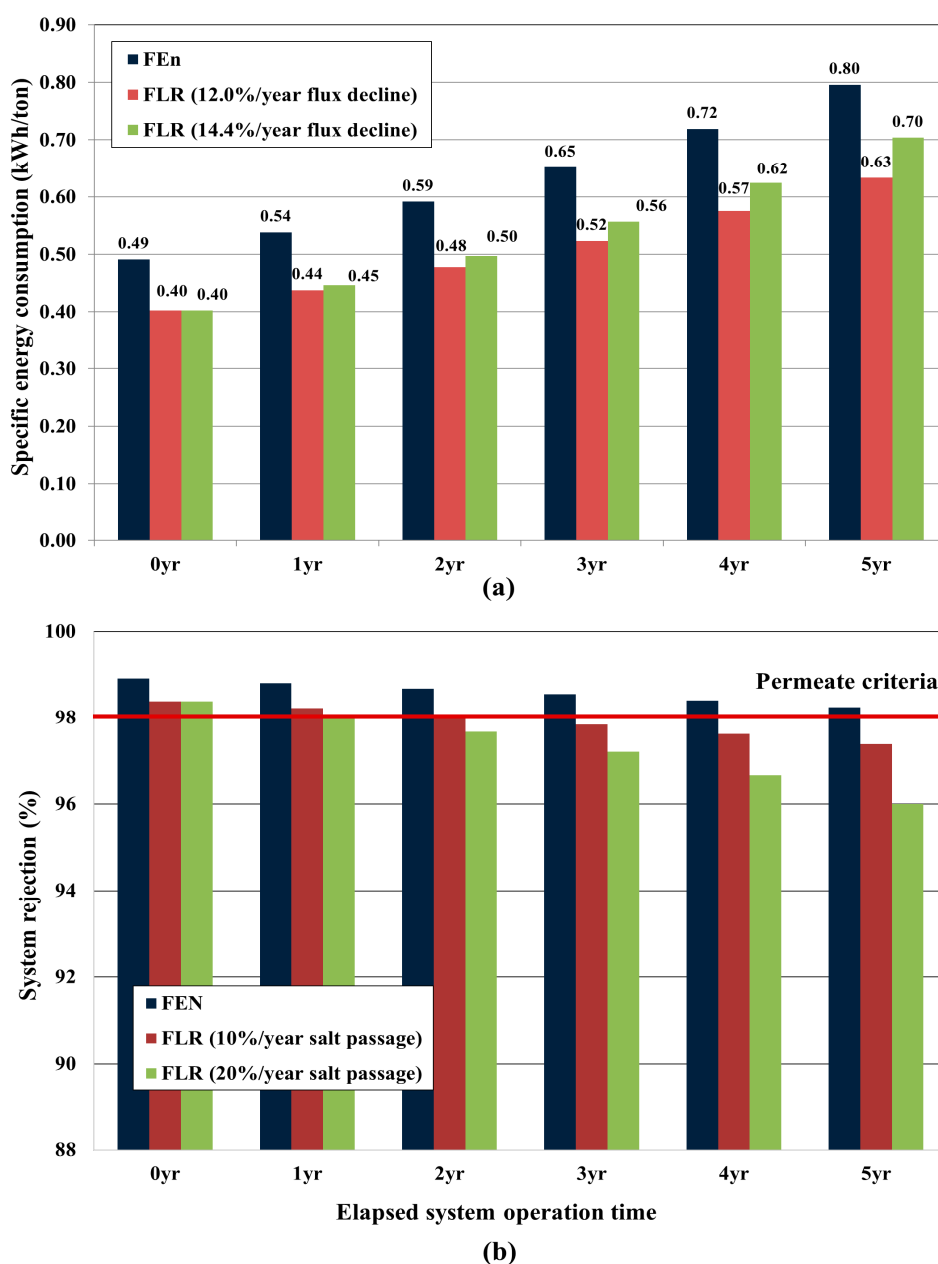


Figure 15. Simulation study results for which the design parameters obtained from pilot test were adopted: (a) Predicted specific energy consumption (kWh) comparison as to the elapsed operation time; (b) Predicted system rejection comparison as to the elapsed operation time.

Table 8. Required quantity of LPRO FLR elements to meet the designated permeate water criteria 98% system salt rejection.

Simulation Study Cases	Replacement Year	No. of Replaced Elements	Element Average Age after Partial Replacement
20%/year annual salt passage increase case	2nd year	2025 EA (83.3%)	1.2 year
10%/year annual salt passage increase case	3rd year	1025 EA (50.0%)	2 year

4. Conclusions

In this study, the feasibility of low-pressure (high flow rate) RO elements was evaluated through the adoption of feed water with a high fouling potential and two types of commercial RO elements with different permeate flow rates. Both the FEn and FLR membranes exhibited quite similar surface characteristics with the only exception of permeability. The initial operating pressure difference at the beginning of the operation clearly originated from the intrinsic flow rate difference between the two RO elements. However, the operating pressure difference became diminished as the membrane fouling progressed. The continuous decrease of the normalized permeate flow (NPF) became larger according to the operation time due to the accumulative membrane fouling, and the degree of permeability decrease is more pronounced for the FLR vessel. The normalized salt passage (NSP) difference between the two vessels started to become larger just after the initial operation start-up point. The salt passage variation rate (SVR) of the FLR vessel was maintained at approximately 2.0 to 2.5 times higher during the entire operation period.

Due to the higher permeability of the FLR membrane, the lead position element of the FLR vessel operated at a higher average flux compared with the FEn case, which led to a localized working load and an intensified membrane fouling. The individual RO element retest results, along with the instrumental analysis for the membrane coupons and foulants, further confirmed the more localized and intensified fouling in the FLR adopted case. The localization of fouling load within a pressure vessel in the LPRO applying case caused about 20% higher flux decline and almost 2-times higher salt passage inclination tendency than those of standard RO membranes. The RO system design simulation study with the adjustment of software input variables predicted that the energy saving capacity of LPRO membranes, which can be expressed as average operating pressure difference ratio (%) between two membranes, decreased from 24.4% to 17.8% and a substantial quantity of LPRO elements (83.3%) must be replaced to meet the designated water criteria only after 2 years operation. So, the LPRO application for high fouling potential feed water needs to be determined with a careful consideration regarding the total operation and maintenance (O&M) cost.

Acknowledgments: This study was supported by the National Research Foundation (NRF) of Korea as funded by the Ministry of Education, Science and Technology (NRF-2015R1D1A1A01058737, NRF-2013R1A1A2004642). The authors are thankful for the support.

Author Contributions: Hyung-Gyu Park conceived, designed, and carried out membrane and RO element performance evaluation, simulation study, pilot test result analysis, and wrote the manuscript; Young-Nam Kwon contributed to the research design, data analysis and presentation, and the writing of the manuscript.

Conflicts of Interest: The authors declare no conflict of interest.

References

1. Cadotte, J.E.; King, R.S.; Majerle, R.J.; Petersen, R.J. Interfacial synthesis in the preparation of reverse osmosis membranes. *J. Macromol. Sci. Chem.* **1981**, *A15*, 727–755. [[CrossRef](#)]
2. Kesting, R.E. *Synthetic Polymeric Membranes*; McGraw-Hill Book Company: New York, NY, USA; St. Louis, MO, USA; San Francisco, CA, USA, 1971.
3. Roh, I.J. Influence of rupture strength of interfacially polymerized thin-film structure on the performance of polyamide composite membranes. *J. Membr. Sci.* **2002**, *198*, 63–74. [[CrossRef](#)]
4. Karode, S.K.; Kulkarni, S.S.; Suresh, A.K.; Mashelkar, R.A. New insights into kinetics and thermodynamics of interfacial polymerization. *Chem. Eng. Sci.* **1998**, *53*, 2649–2663. [[CrossRef](#)]
5. Son, M.; Park, H.; Liu, L.; Choi, H.; Kim, J.H.; Choi, H. Thin-film nanocomposite membrane with CNT positioning in support layer for energy harvesting from saline water. *Chem. Eng. J.* **2016**, *284*, 68–77. [[CrossRef](#)]
6. Venkata Swamy, B.; Madhumala, M.; Prakasham, R.S.; Sridhar, S. Nanofiltration of bulk drug industrial effluent using indigenously developed functionalized polyamide membrane. *Chem. Eng. J.* **2013**, *233*, 193–200. [[CrossRef](#)]
7. Byrne, W. *Reverse Osmosis*, 2nd ed.; Tall Oaks Publishing Inc.: Littleton, CO, USA, 1995.

8. Kucera, J. *Reverse Osmosis*; John Wiley & Sons: Hoboken, NJ, USA, 2010.
9. Mulder, M. *Basic Principles of Membrane Technology*, 2nd ed.; Kluwer Academic Publishers: Dordrecht, The Netherlands, 1996.
10. Kwon, Y.-N.; Hong, S.; Choi, H.; Tak, T. Surface modification of a polyamide reverse osmosis membrane for chlorine resistance improvement. *J. Membr. Sci.* **2012**, *415–416*, 192–198. [[CrossRef](#)]
11. Hasson, D.; Shemer, H.; Brook, I.; Zaslavski, I.; Semiat, R.; Bartels, C.; Wilf, M. Scaling propensity of seawater in RO boron removal processes. *J. Membr. Sci.* **2011**, *384*, 198–204. [[CrossRef](#)]
12. Ghosh, A.K.; Hoek, E.M.V. Impacts of support membrane structure and chemistry on polyamide–polysulfone interfacial composite membranes. *J. Membr. Sci.* **2009**, *336*, 140–148. [[CrossRef](#)]
13. Gu, J.E.; Jun, B.M.; Kwon, Y.N. Effect of chlorination condition and permeability of chlorine species on the chlorination of a polyamide membrane. *Water Res.* **2012**, *46*, 5389–5400. [[CrossRef](#)] [[PubMed](#)]
14. Choi, H.; Park, J.; Tak, T.; Kwon, Y.-N. Surface modification of seawater reverse osmosis (SWRO) membrane using methyl methacrylate-hydroxy poly(oxyethylene) methacrylate (MMA-HPOEM) comb-polymer and its performance. *Desalination* **2012**, *291*, 1–7. [[CrossRef](#)]
15. Hong, S.; Kim, I.-C.; Tak, T.; Kwon, Y.-N. Interfacially synthesized chlorine-resistant polyimide thin film composite (TFC) reverse osmosis (RO) membranes. *Desalination* **2013**, *309*, 18–26. [[CrossRef](#)]
16. Kwon, Y.-N.; Joksimovic, R.; Kim, I.-C.; Leckie, J.O. Effect of bromide on the chlorination of a polyamide membrane. *Desalination* **2011**, *280*, 80–86. [[CrossRef](#)]
17. Xia, S.; Yao, L.; Zhao, Y.; Li, N.; Zheng, Y. Preparation of graphene oxide modified polyamide thin film composite membranes with improved hydrophilicity for natural organic matter removal. *Chem. Eng. J.* **2015**, *280*, 720–727. [[CrossRef](#)]
18. Park, H.-G.; Cho, S.-G.; Kim, K.-J.; Kwon, Y.-N. Effect of feed spacer thickness on the fouling behavior in reverse osmosis process—A pilot scale study. *Desalination* **2016**, *379*, 155–163. [[CrossRef](#)]
19. Li, N.N.; Fane, A.G.; Winston, W.S.; Matsuura, T. *Advanced Membrane Technology and Applications*; John Wiley & Sons, Inc.: Hoboken, NJ, USA, 2008.
20. Huang, H.; Schwab, K.; Jacangelo, J.G. Pretreatment for low pressure membranes in water treatment: A review. *Environ. Sci. Technol.* **2009**, *43*, 3011–3019. [[CrossRef](#)] [[PubMed](#)]
21. Baker, R.W. *Membrane Technology and Applications*, 2nd ed.; John Wiley & Sons: Chichester, UK, 2004.
22. Dalvi, A.G.I.; Al-Rasheed, R.; Javeed, M.A. Studies on organic foulants in the seawater feed of reverse osmosis plants of SWCC. *Desalination* **2000**, *132*, 217–232. [[CrossRef](#)]
23. Kucera, J. *Reverse Osmosis: Design, Processes, and Applications for Engineers*, 2nd ed.; Scrivener Publishing, Wiley: Hoboken, NJ, USA, 2015.
24. Araújo, P.A.; Kruihof, J.C.; Van Loosdrecht, M.C.M.; Vrouwenvelder, J.S. The potential of standard and modified feed spacers for biofouling control. *J. Membr. Sci.* **2012**, *403–404*, 58–70. [[CrossRef](#)]
25. She, Q.; Wang, R.; Fane, A.G.; Tang, C.Y. Membrane fouling in osmotically driven membrane processes: A review. *J. Membr. Sci.* **2016**, *499*, 201–233. [[CrossRef](#)]
26. Wang, Y.-N.; Tang, C.Y. Protein fouling of nanofiltration, reverse osmosis, and ultrafiltration membranes—The role of hydrodynamic conditions, solution chemistry, and membrane properties. *J. Membr. Sci.* **2011**, *376*, 275–282. [[CrossRef](#)]
27. Choi, H.; Jung, Y.; Han, S.; Tak, T.; Kwon, Y.-N. Surface modification of SWRO membranes using hydroxyl poly(oxyethylene) methacrylate and zwitterionic carboxylated polyethyleneimine. *J. Membr. Sci.* **2015**, *486*, 97–105. [[CrossRef](#)]
28. Kwon, Y.-N.; Shih, K.; Tang, C.; Leckie, J.O. Adsorption of perfluorinated compounds on thin-film composite polyamide membranes. *J. Appl. Polym. Sci.* **2012**, *124*, 1042–1049. [[CrossRef](#)]
29. Bacchin, P.; Aimar, P.; Field, R.W. Critical and sustainable fluxes: Theory, experiments and applications. *J. Membr. Sci.* **2006**, *281*, 42–69. [[CrossRef](#)]
30. Drews, A. Membrane fouling in membrane bioreactors—Characterisation, contradictions, cause and cures. *J. Membr. Sci.* **2010**, *363*, 1–28. [[CrossRef](#)]
31. Le-Clech, P.; Chen, V.; Fane, T.A.G. Fouling in membrane bioreactors used in wastewater treatment. *J. Membr. Sci.* **2006**, *284*, 17–53. [[CrossRef](#)]
32. Tang, C.Y.; Chong, T.H.; Fane, A.G. Colloidal interactions and fouling of NF and RO membranes: A review. *Adv. Colloid Interface Sci.* **2011**, *164*, 126–143. [[CrossRef](#)] [[PubMed](#)]

33. Norberg, D.; Hong, S.; Taylor, J.; Zhao, Y. Surface characterization and performance evaluation of commercial fouling resistant low-pressure RO membranes. *Desalination* **2007**, *202*, 45–52. [[CrossRef](#)]
34. Zhao, L.; Chang, P.C.Y.; Yen, C.; Ho, W.S.W. High-flux and fouling-resistant membranes for brackish water desalination. *J. Membr. Sci.* **2013**, *425–426*, 1–10. [[CrossRef](#)]
35. Louie, J.S.; Pinnau, I.; Ciobanu, I.; Ishida, K.P.; Ng, A.; Reinhard, M. Effects of polyether–polyamide block copolymer coating on performance and fouling of reverse osmosis membranes. *J. Membr. Sci.* **2006**, *280*, 762–770. [[CrossRef](#)]
36. Gilron, J.; Belfer, S.; Väisänen, P.; Nyström, M. Effects of surface modification on antifouling and performance properties of reverse osmosis membranes. *Desalination* **2001**, *140*, 167–179. [[CrossRef](#)]
37. Belfer, S.; Purinson, Y.; Fainshtein, R.; Radchenko, Y.; Kedem, O. Surface modification of commercial composite polyamide reverse osmosis membranes. *J. Membr. Sci.* **1998**, *139*, 175–181. [[CrossRef](#)]
38. Freger, V.; Gilron, J.; Belfer, S. TFC polyamide membranes modified by grafting of hydrophilic polymers: An FT-IR/AFM/TEM study. *J. Membr. Sci.* **2002**, *209*, 283–292. [[CrossRef](#)]
39. Toray Chemical Korea Inc. *CSM Technical Manual*; Toray Chemical Korea Inc.: Seoul, Korea, 2008.
40. Xie, M.; Nghiem, L.D.; Price, W.E.; Elimelech, M. Impact of organic and colloidal fouling on trace organic contaminant rejection by forward osmosis: Role of initial permeate flux. *Desalination* **2014**, *336*, 146–152. [[CrossRef](#)]
41. Miller, D.J.; Kasemset, S.; Paul, D.R.; Freeman, B.D. Comparison of membrane fouling at constant flux and constant transmembrane pressure conditions. *J. Membr. Sci.* **2014**, *454*, 505–515. [[CrossRef](#)]
42. Tang, C.Y.; Kwon, Y.-N.; Leckie, J.O. The role of foulant–foulant electrostatic interaction on limiting flux for RO and NF membranes during humic acid fouling—Theoretical basis, experimental evidence, and AFM interaction force measurement. *J. Membr. Sci.* **2009**, *326*, 526–532. [[CrossRef](#)]
43. Kwon, Y.-N.; Leckie, J.O. Hypochlorite degradation of crosslinked polyamide membranes: I. Changes in chemical/morphological properties. *J. Membr. Sci.* **2006**, *283*, 21–26. [[CrossRef](#)]
44. Kwon, Y.-N.; Leckie, J.O. Hypochlorite degradation of crosslinked polyamide membranes: II. Changes in hydrogen bonding behavior and performance. *J. Membr. Sci.* **2006**, *282*, 456–464. [[CrossRef](#)]
45. Chun, Y.; Zaviska, F.; Kim, S.-J.; Mulcahy, D.; Yang, E.; Kim, I.S.; Zou, L. Fouling characteristics and their implications on cleaning of a FO-RO pilot process for treating brackish surface water. *Desalination* **2016**, *394*, 91–100. [[CrossRef](#)]
46. Kim, S.-J.; Oh, B.S.; Yu, H.-W.; Kim, L.H.; Kim, C.-M.; Yang, E.-T.; Shin, M.S.; Jang, A.; Hwang, M.H.; Kim, I.S. Foulant characterization and distribution in spiral wound reverse osmosis membranes from different pressure vessels. *Desalination* **2015**, *370*, 44–52. [[CrossRef](#)]
47. Toray Chemical Korea Inc. Csmpro 5.0. Available online: <http://www.Csmfilter.Com/> (accessed on 2 March 2017).
48. Dow Chemical Company. Rosa. Available online: <http://www.Dow.Com/en-us/water-and-process-solutions/resources/design-software> (accessed on 8 April 2017).
49. Hydranautics. Imsdesign. Available online: <http://membranes.Com/solutions/software/> (accessed on 8 April 2017).
50. Toray Industries Inc. Ds2. Available online: <https://ap3.Toray.Co.Jp/toraywater/> (accessed on 8 April 2017).

